Thermotropic Polymorphism of a Nonphospholipid Mixture: Lactylated Fatty Acid Esters of Glycerol and Propylene Glycol

Ingrid Winter[a,*], Karl Lohner[b], Hans-Gerd M. Janssen[a], and Sergey M. Mel'nikov[a]

[a]Foods Research Centre, Unilever R&D Vlaardingen, 3133 AT Vlaardingen, The Netherlands, and [b]Institute of Biophysics and X-ray Structure Research, Austrian Academy of Sciences, A-8042 Graz, Austria

ABSTRACT: Lactylated FA esters of glycerol and propylene glycol (LFEGPG) are a lipid blend that is commercially available and used in the food industry as an emulsifying agent. Because the mutual impact of the two different backbones on the lipid phase behavior was of particular interest, we fractionated the commercial lipid blend by column LC. Fractions with varying ratios of glycerol and propylene glycol esters were collected and characterized by MS. DSC and X-ray diffraction were applied to study the thermotropic phase behavior of the dry emulsifier and the derived lipid fractions. LFEGPG exhibited rich polymorphic behavior, adopting a sub-α-crystalline phase that converted to an α-crystalline phase. Concomitantly, a β-crystalline phase was formed by some components of this lipid mixture. We found that the fractions with the highest amounts of lipids bearing the less-polar propylene glycol as their backbone tended to form a β-crystalline phase. Also, a higher number of self-polymerized lactic acid molecules in the head group of the propylene glycol esters favored the formation of a β-crystalline phase.

Paper no. J10886 in *JAOCS 81*, 961–969 (October 2004).

KEY WORDS: Chromatography, differential scanning calorimetry, food-grade emulsifier, lamellar crystalline phases, mass spectrometry, X-ray diffraction.

A range of synthetic nonphospholipids (NPL), prevalently MAG, DAG, and derivatives thereof, are used in the food industry as legally approved surfactants for the preparation of emulsions and microemulsions (1,2). Furthermore, the use of synthetic NPL as alternatives to conventional phospholipids (PL) in various applications is a promising strategy because of the exceptional advantages of NLP, namely, their ease of manufacture, stability, versatility (3), stability against phospholipases *in vivo* (4), and affordability. At present, the phase behavior of most of these food emulsifiers is poorly characterized. To fill this gap and to extend our understanding of the phase behavior of NPL derived from a food-grade source, we studied a mixture of lactylated FA esters of glycerol and propylene glycol (LFEGPG) that is commercially available, e.g., under the name Durlac 300. In this lipid blend, the esterified FA are mainly palmitic and stearic acids. In addition to examining the thermotropic phase behavior of the solid LFEGPG sample, it was of particular interest to understand how the different lipid backbones, glycerol and propylene glycol, mutually influence the lipid phase behavior. Therefore, we fractionated the commercial lipid blend by column LC and collected fractions with increased amounts of lactylated propylene glycol esters.

No literature is available on the phase behavior of the LFEGPG blend. However, one of its basic structural constituents, MAG, is known to exhibit rich polymorphic behavior. When solidified from the melted state, a thermodynamically unstable α-crystalline phase with hexagonally packed hydrocarbon chains is formed, but it converts within a short time interval to a stable β-crystalline phase with triclinically packed chains (2,5). Systematic studies of the polymorphic phase behavior of pure palmitic and stearic acid esters of propylene glycol were performed by Martin and Lutton (6) and Lutton *et al.* (7). Although there is some confusion regarding the nomenclature of the phases described in these publications, the thermotropic phase behavior seems comparable to that of free MAG, exhibiting a metastable α-crystalline form. Because a metastable α-crystalline form is undesirable in food emulsions, a method to avoid the undesirable phase conversions and to stabilize MAG in their α-crystalline form was singled out (8). It was found that in a nearly equimolar mixture of monostearoylglycerol and monostearoylpropylene glycol, named "conjoined crystals" (8), a substantial portion of the glycerol esters was in the α-crystalline phase. Whereas the α-crystalline form of the MAG was stable for extended periods of time, the esters of propylene glycol changed from the α-form to the β′-form with orthorhombically packed hydrocarbon chains within a short time interval.

The free hydroxyl groups of the FA esters of glycerol and propylene glycol can be esterified with lactic acid, leading to LFEGPG. The esterification of the head group decreases the lipid polarity and reduces the melting temperature by at least 10°C as compared with nonlactylated lipids, depending on the precise formulation of the "conjoined crystals" (8). The preparation of such lactylated mixed esters is described in U.S. Patent 3,158,487 (9). In the preferred method, TAG react with a mixture of glycerol and propylene glycol, after which

*To whom correspondence should be addressed at Foods Research Centre, Unilever R&D Vlaardingen, Olivier van Noortlaan 120, 3133 AT Vlaardingen, The Netherlands. Email: ingrid.winter@unilever.com

lactic acid is added slowly to esterify the free hydroxyl groups in the mixed esters. Fully lactylated esters are produced only when lactic acid is added in excess. Depending on the rate of lactic acid addition, lactic acid polymers are formed during the reaction (5,9).

MATERIALS AND METHODS

LFEGPG (Durlac 300) was obtained from Loders Crocklaan (Channahon, IL). All organic solvents were of HPLC grade. Silica gel (60–200 mesh, pore size 150 Å) for the column LC was from J.T.Baker (Deventer, The Netherlands).

The separation of individual components from the LFEGPG blend (Durlac 300) was performed by HPLC on a Zorbax 5SI/EM2 silica column, 100 × 3.0 mm i.d. (Agilent Technologies Netherlands B.V., Amstelveen, The Netherlands), at 34°C and a flow rate of 0.6 mL/min, with an eluent system featuring increasing polarity (Table 1). The fractions were detected by ELSD (ELSD IIA detector; Alltech, Deerfeeld, IL) at a drift tube temperature of 98.4°C, a N_2 flow of 60 mm (flow meter), and a pressure of 51 psi.

Based on the results of the HPLC experiments, the following procedure was developed for the preparative separation of the LFEGPG sample by column LC. Durlac 300 (90 g) was dissolved in 1.7 L of hexane and loaded onto a column packed with activated silica gel. The bed volume was 1.7 L. Elution of the sample from the stationary phase was performed with a gradient system of hexane and 2-propanol (IPA) with increasing IPA content as follows: 4 × 1.7 L of hexane + 2% IPA; 4 × 1.7 L of hexane + 5% IPA; 4 × 1.7 L of hexane + 20% IPA. The entire separation was performed within 3 h. MS data showed that from the 12 fractions collected, the fractions 5, 6, and 7 were highly enriched in propylene glycol esters; consequently, they were used for further investigations. The separation procedure was reproducible, as demonstrated by MS results.

TABLE 1
Eluent Gradient Used for the Separation of Lactylated FA Esters of Glycerol and Propylene Glycol (LFEGPG) (Durlac 300) by HPLC

Time (min)	A[a] (%)	B[b] (%)	C[c] (%)	Flow rate (mL/min)
0	100	0	0	0.6
10	100	0	0	0.6
20	82	18	0	0.6
35	56	40	4	0.6
38	38	54	8	0.6
45	35	55	10	0.6
57	32.5	56	11.5	0.6
70	16	56	28	0.6
70.1	30	70	0	0.6
72	30	70	0	0.6
75	30	70	0	1.4
80	100	0	0	1.4
90	100	0	0	1.4
95	100	0	0	0.6
102	100	0	0	0.6
105	100	0	0	0

[a]Hexane/tetrahydrofuran (99:1, vol/vol).
[b]Chloroform/2-propanol (1:4, vol/vol).
[c]2-Propanol/H_2O (0.53 M NH_3) (1:1, vol/vol).

All MS measurements were carried out on a Quattro-II triple quadrupole mass spectrometer (Micromass UK Ltd., Manchester, United Kingdom). For the MS analysis, 100 µL of each fraction was mixed with 600 µL of dichloromethane and 300 µL of a 1-mM sodium iodide solution in a mixture of methanol and ethanol at a ratio of 1:1 (vol/vol). For tandem MS (MS-MS) analyses, the sodium iodide solution was replaced with a 300-mM ammonium acetate solution in methanol. All fractions were analyzed using direct-introduction MS in positive electrospray mode, at a capillary voltage of 4 kV, a cone voltage of 55 V, and using a scan range of 100–1200 amu. The ions of interest detected in the full-scan analysis were analyzed using MS-MS. The collision gas used was argon at a pressure of $6.9.10^{-4}$ mbar. The collision energy was ramped from 32.6 to 8.2 eV over a mass range of 50 to 750 amu.

DSC heating and cooling scans were performed with a temperature-modulated differential scanning calorimeter (PerkinElmer DSC Pyris 1; PerkinElmer Instruments, Shelton, CT). Amounts of 5 to 10 mg of the dry lipid samples were accurately weighed and sealed in aluminum sample pans. As a reference, an empty sample pan was used. Samples were thermally equilibrated for 30 min at 0°C before starting the heating scans. All heating and cooling scans were recorded at a scan rate of 5°C/min. Heating and cooling thermograms were recorded at temperatures between 0 and 70°C (LFEPGP and fraction 5) and between 0 and 80°C (fractions 6 and 7). Data were analyzed using the Pyris software provided by PerkinElmer. The heat flow was normalized to the amount of lipid analyzed, and the calorimetric enthalpies were calculated by integrating the peak areas after baseline adjustment. The thermograms were finalized with Origin software (MicroCal Inc., Northampton, MA).

X-ray diffraction patterns were recorded simultaneously in the small- and wide-angle regions using a SWAX-camera (Hecus X-ray Systems, Graz, Austria) mounted on a sealed-tube generator (Seifert, Ahrensburg, Germany) operating at 50 kV and 40 mA. Cu K_α radiation (λ = 1.542 Å) was selected using a Ni filter (10). Solid samples were fixed between two polyethylene terephthalate films (Kalle Austria GmbH, Guntramsdorf, Austria) in a paste sample holder, and the temperature was controlled using a Peltier unit (Hecus X-ray Systems). Calibration was performed in the small-angle region with silver stearate and in the wide-angle region with a *p*-bromobenzoic acid standard, respectively. Samples were thermally equilibrated for 30 min at 5°C and for 15 min at the higher temperatures before initiating data acquisition. The samples were heated to temperatures at least 10°C above the main phase transition, except for fraction 7, because of the limited temperature range (1 to 65°C) of the instrument, and then cooled back to 5°C. Exposure times of 2000 s were chosen for both the small- and the wide-angle regions.

RESULTS AND DISCUSSION

Figure 1 depicts the MS spectrum of the LFEGPG (Durlac 300) sample. The esterified FA are stearic acid (C18:0) and,

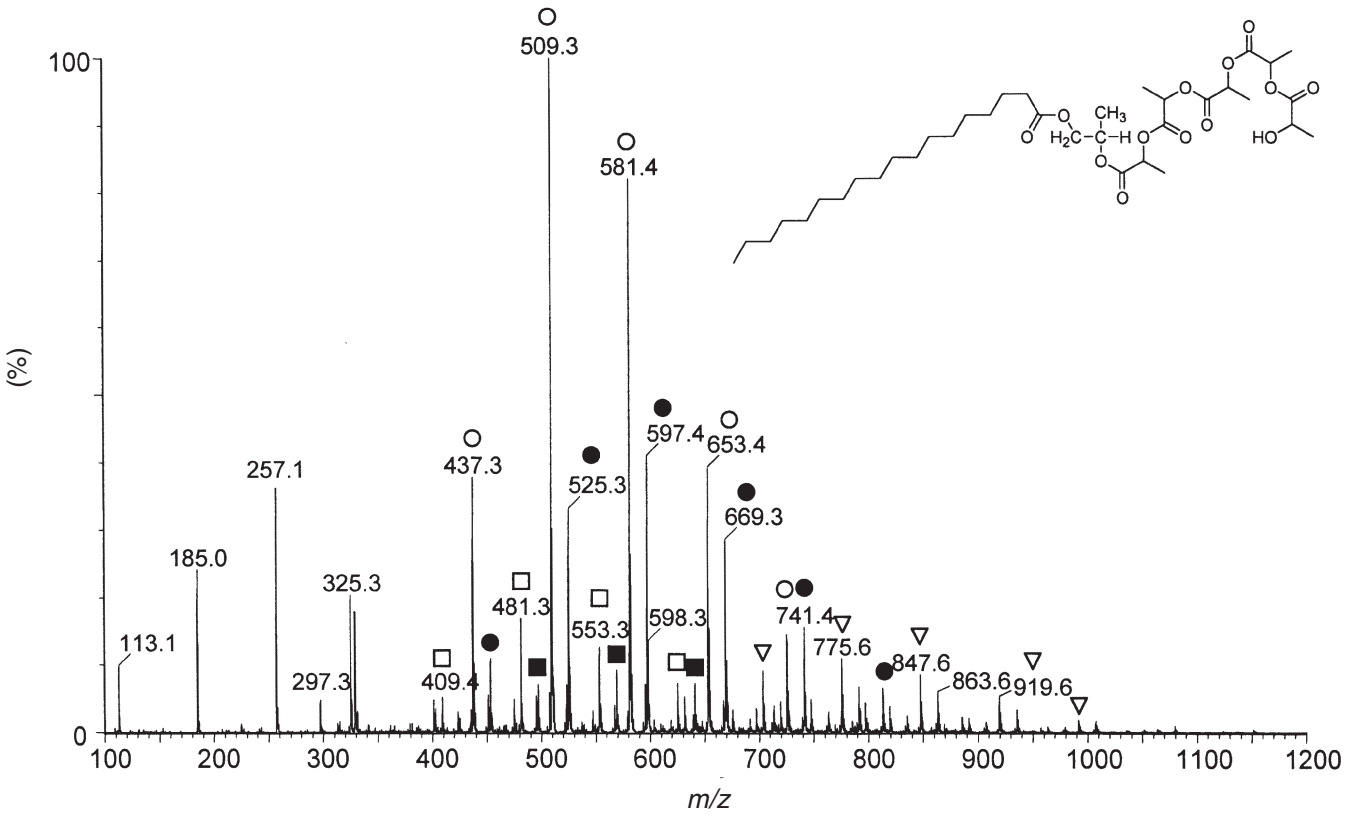

FIG. 1. Mass spectrum of the lactylated FA esters of glycerol and propylene glycol (LFEGPG) blend (Durlac 300; Loders Crocklaan, Channahon, IL). The *m/z* ratios indicated were assigned to the following compounds: propylene glycol esters of one FA (C18:0) and one to six lactic acid units (○); glycerol esters of one FA (C18:0) and one to seven lactic acid units (●); propylene glycol esters of one FA (C16:0) and one to five lactic acid units (□); glycerol esters of one FA (C16:0) and one to five lactic acid units (■); glycerol esters of two FA (C18:0) and zero to six lactic acid units (▽); *m/z* ratios between 113 and 325 were assigned to lactic acid and lactic acid polymers (one to four units). The inset shows the main component of LFEGPG, which consists of a C16:0 or C18:0 FA that is esterified to 1,2-propanediol. Its lactic acid moiety consists of up to six lactic acid molecules.

to a minor extent, palmitic acid (C16:0). Because single lactic acid molecules can form polylactic acid, up to seven lactic acid molecules per lipid molecule were detected. Lactylated stearic acid esters of propylene glycol with one FA and one to six lactic acid molecules were found to be the main component of Durlac 300 (Fig. 1, inset). Further components identified are given in the caption of Figure 1.

The investigation of Durlac 300 by HPLC was based on the increasing polarity of the eluent. With this method, it was possible to separate lipid fractions of different polarity according to the number of OH-groups. Three fractions were obtained at retention times of 3, 21, and 24 min that were characteristic of compounds bearing zero, one, and two free OH-groups, respectively. The preparative separation of LFEGPG into fractions with an increased content of propylene glycol esters, as revealed by MS investigations, in a single-step approach was performed by using column LC. Table 2 gives the components of the fractions derived from column LC. Fraction 5 was the least polar of the three fractions collected and consisted mainly of esters bearing two FA and between zero and six lactic acid units. Approximately 7% of this fraction was composed of glycerol esters. The amount of glycerol esters was as low as approximately 3% in fraction 6. The main components of fraction 6 were propylene glycol esters of a FA and a lactic acid unit consisting of up to five lactic acid molecules. Among these three fractions, fraction 7 had the highest polarity. Its main components were propylene glycol esters of one FA and a lactic acid ester with a maximum of six lactic acid molecules. The amount of glycerol esters was nearly equal to 3%. For comparison, the percentage of glycerol esters in LFEGPG was determined to be 18%. These values represent the percentage of all lactylated glycerol ester ions in the total amount of ions present in the spectrum. These are, however, only estimated percentages, as no correction was carried out for differences in the ionization responses. Monomers and polymers of lactic acid were detected in all fractions. However, glycerol esters with two free OH-groups were successfully removed, and only glycerol esters bearing two FA esters plus lactic acid esters were present in the fractions studied. Because fractions 5, 6, and 7 exhibited increasing polarity, the polarity of the lipid molecules obviously increased with an increasing number of lactic acid molecules in the head group when the hydrocarbon chain length remained the same (see Table 2).

The thermotropic phase behavior of LFEGPG and behavior of the three fractions derived from it (fractions 5, 6, and

TABLE 2
Composition of Fractions 5, 6, and 7 as Determined by MS

Sample[a]	*m/z* range	Structure
Fraction 5		
1	631–991	Propylene glycol + 2 C18:0 + 0–6 lactic acid esters
2	437–581	Propylene glycol + 1 C18:0 + 1–3 lactic acid esters
3	603–963	Propylene glycol + 1 C16:0 + 1 C18:0 + 0–5 lactic acid esters
4	647–935	Glycerol + 2 C18:0 + 0–4 lactic esters + small amount of propylene glycol + 2 C16:0 + 0–6 lactic acid esters
5	113–257	Lactic acid mono- and polymers, 1–3 units
6	619–907	Glycerol + 1 C16:0 + 1 C18:0 + 0–4 lactic acid esters
Fraction 6		
1	437–725	Propylene glycol + 1 C18:0 + 1–5 lactic acid esters
2	113–325	Lactic acid mono- and polymers, 1–4 units
3	409–625	Propylene glycol + 1 C16:0 + 1–4 lactic acid esters
Fraction 7		
1	437–797	Propylene glycol + 1 C18:0 + 1–6 lactic acid esters
2	481–697	Propylene glycol + 1 C16:0 + 2–4 lactic acid esters
3	113–325	Lactic acid mono- and polymers, 1–4 units

[a]Compounds within a fraction are listed in decreasing intensity.

7) are illustrated by their DSC scans (Fig. 2). The heat capacity changes observed with the transitions are listed in Table 3. Upon heating, all samples except fraction 5 exhibited a lower enthalpic (~0.4–0.7 J/g) phase transition at about 7 to 9°C. The X-ray diffractograms (see the following discussion) showed that these transitions were due to changes in the hydrocarbon chain packing involving a reorganization from an orthorhombic to a hexagonal packing. Upon cooling, these small low-temperature peaks were not observed. However, after 30 min of incubation at 0°C, these phase transitions could be observed again upon heating (data not shown). All samples exhibited an endothermic phase transition around 40°C because of the hydrocarbon chain melting of the α-crystalline phase and transition into the isotropic liquid phase, as revealed by the X-ray diffractograms. LFEGPG exhibited a chain-melting transition at 40.9°C, with a transition enthalpy of 83 J/g. A small peak with the maximum at 47.4°C overlapped with the main transition peak. Deconvolution of the normalized excess heat capacity function showed that this small peak exhibited an enthalpy of about 1 J/g. Fraction 5 exhibited one endothermic phase transition, with the heat capacity maximum at 42.2°C. Compared with the crude sample, the transition temperature of this fraction was shifted to higher temperatures by about one degree, and its enthalpy was significantly increased. Fraction 6 showed a hydrocarbon chain-melting transition at 39.6°C, followed by a low enthalpic transition at about 53°C. Unlike in the crude sample, this transition at the higher temperature was completely separated from the main transition. The thermogram of fraction 7 showed two transitions at elevated temperatures, the first with the maximum at 38.6°C and the second with the maximum at 65.5°C. The sum of the enthalpies of the two peaks was somewhat smaller than the enthalpy of the LFEGPG main transition. Hence, in fractions 6 and 7 the maximum of the first chain-melting event on heating was occurring at temperatures slightly below the main chain-melting temperature of the crude sample, whereas the second peak occurred at much higher temperatures. The X-ray diffraction data revealed that the higher-temperature endotherm could be assigned to the melting of a β-crystalline phase.

The main transitions were reversible upon cooling, albeit at about 5–6°C lower temperatures. Only the cooling curve of fraction 5 exhibited the same shape as the heating curve. With the LFEGPG blend and fraction 7, additional shoulders were occurring, whereas in fraction 6 the mode of recrystallization seemed to be different compared with the mode of melting, since the small peak at high temperatures was abolished and the crystallization occurred in one event. These differences upon cooling were probably due to the kinetics of formation of the various crystalline phases, similar to Blaurock's (11) description of the cooling scans of TAG. Blaurock described the appearance of the different crystallization exotherms as being highly dependent on the applied scan rate. Because the formation of α-crystals takes place most rapidly, there might be insufficient time for the formation of β-crystals before the temperature drops below the melting temperature of the α-crystals at high scan rates. Only when the cooling rate is slow enough can the β-crystals form before the α-melting temperature is reached. The latter was obviously the case for fraction 7, whereas in fraction 6 the temperature difference between the two m.p. was so small that β-crystallization occurred at lower temperatures and α-crystallization was therefore superimposed on it. However, X-ray diffraction revealed the reversibility of the lattice spacings for all samples.

The X-ray diffractograms obtained were rather complicated because of the inhomogeneity of the samples. In the small-angle region, each sample exhibited several sharp Bragg reflections below the hydrocarbon chain-melting temperature (Table 4). Taking into account that LFEGPG is a mixture of various components, it is probable that the different components of the sample formed different crystalline phases. The coexistence of different phases over a wide temperature range also has been observed in fat samples, e.g., in palm stearin (12). However, indexing of the peak positions

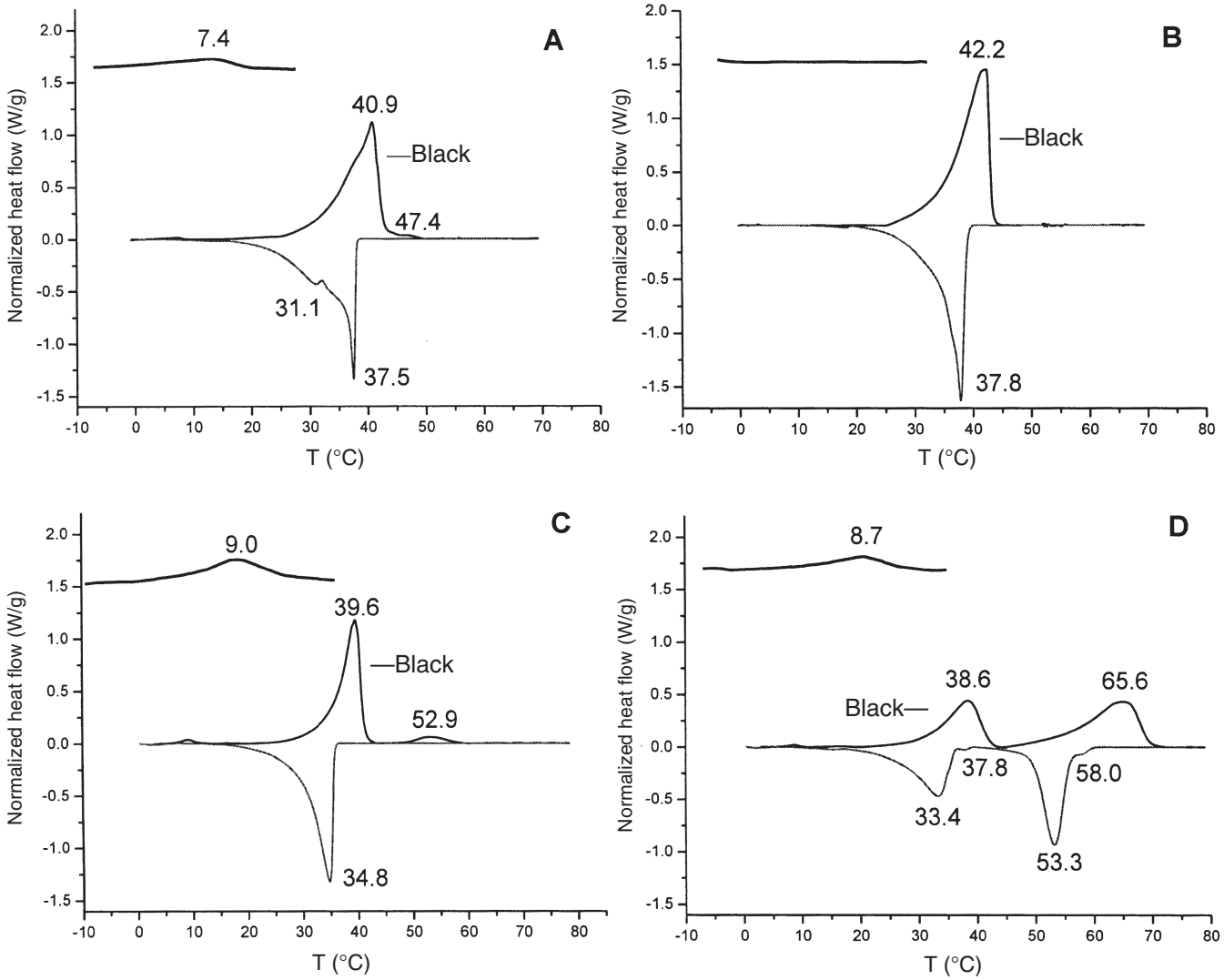

FIG. 2. DSC thermograms of the solid LFEGPG and fractions derived from it: heating (black lines) and cooling (gray lines) scans of LFEGPG (A), fraction 5 (B), fraction 6 (C), and fraction 7 (D). Inserts show the enlarged heating scans in the low-temperature range. Transition temperatures are indicated within the figure. For abbreviation see Figure 1.

TABLE 3
Thermodynamic Characterization of the Thermotropic Phase Transitions of the LFEGPG Blend and the Fractions Derived from It

Sample	Transition temperature (°C)	Transition enthalpy (J/g)	Transition type[a]
LFEGPG	7.4	~0.5	$Lc_{sub\text{-}\alpha}/Lc_{\alpha}$
LFEGPG	40.9	83	Lc_{α}/Fl
LFEGPG	47.4	1	Lc_{β}/Fl
Fraction 5	42.2	105	Lc_{α}/Fl
Fraction 6	9.0	~0.7	$Lc_{sub\text{-}\alpha}/Lc_{\alpha}$
Fraction 6	39.6	61	Lc_{α}/Fl
Fraction 6	52.9	5	Lc_{β}/Fl
Fraction 7	8.7	~0.4	$Lc_{sub\text{-}\alpha}/Lc_{\alpha}$
Fraction 7	38.6	36	Lc_{α}/Fl
Fraction 7	65.6	45	Lc_{β}/Fl

[a]Transition types were assigned by X-ray diffraction data. $Lc_{sub\text{-}\alpha}$, sub-α-crystalline phase; Lc_{α}, α-crystalline phase; Lc_{β}, β-crystalline phase; Fl, isotropic fluid phase; for other abbreviation see Table 1.

showed that almost all Bragg peaks could be assigned to a 1-D lamellar lattice, which gave rise to spacing ratios of 1:2:3. The wide-angle patterns provided information on the lateral hydrocarbon chain packing. Generally, one can distinguish three main types of polymorphic crystal chain packing in solid lipid or fat samples, the α, β′, and β forms, which exhibit increasing stability in this order. The α-crystalline phase, with a hexagonally packed subcell, is characterized by a single peak located at about 4.2 Å. An orthorhombic subcell (β′-crystalline phase and sub-α-crystalline phase, respectively) gives rise to an additional weak reflection at about 3.8 Å. An additional Bragg peak at about 4.6 Å can be assigned to a triclinical crystalline subcell (β-crystalline phase) (13). The wide-angle diffractograms of a melted lipid sample in the isotropic liquid phase exhibit a broad diffuse reflection at about 4.6 Å (14).

The small- and wide-angle diffractograms of fraction 6 (Fig. 3) demonstrated the coexistence of two lamellar structures,

TABLE 4
Reflections Observed in the X-ray Diffractograms in the SAXS and WAXS Regions

	SAXS				WAXS				
LFEGPG									
5°C	**61.4**	54.4	46.2	**34.1**	4.6	**4.18**	3.82		
20°C	**61.4**	54.4	46.2	**34.1**	4.6	**4.12**			
40°C		54.4			4.6				
55°C		*51.6*							
5°C	**59.6**	51.6			4.6	4.19	3.82		
Fraction 5									
5°C	**58.3**	46.5			4.25	**4.17**		3.77	
20°C	**57.9**	46.8			4.30	**4.17**	4.13	3.80	
40°C	**52.2**					*4.18*	*3.83*	*3.73*	
55°C									
5°C	**56.7**					**4.14**			
Fraction 6									
5°C	**51.2**	**33.4**	30.4		4.6	**4.19**	**3.81**	*3.65*	
20°C	**51.2**	**33.3**			4.6	**4.12**	*3.86*	*3.67*	
40°C	**51.6**				4.6		*3.89*	*3.69*	
55°C	**51.6**				4.6		*3.89*	*3.69*	
65°C									
5°C	**51.2**	**33.4**			4.6	**4.19**	3.82	*3.64*	*3.59*
Fraction 7									
5°C	**54.4**	51.2	**33.8**	30.5	**4.6**	**4.19**	**3.80**	**3.64**	*3.59*
20°C	**54.4**	51.2	**33.7**		**4.6**	**4.12**	**3.80**	**3.68**	*3.61*
							3.89		
40°C	**54.4**	51.2			**4.6**		**3.81**	**3.73**	*3.64*
							3.90		
55°C	**54.4**	51.2			**4.6**		**3.81**	**3.76**	3.65
						3.93			*3.71*
65°C	**54.4**				**4.6**			3.83	3.78
5°C	**54.4**		**34.8**	30.4	**4.6**	**4.19**	**3.76**	*3.70*	

[a]All spacings are given in Angstroms. Bold letters indicate spacings related to the strong reflections, italic letters to spacings of the weak reflections. SAXS, small-angle X-ray scattering; WAXS, wide-angle X-ray scattering; for other abbreviation see Table 1.

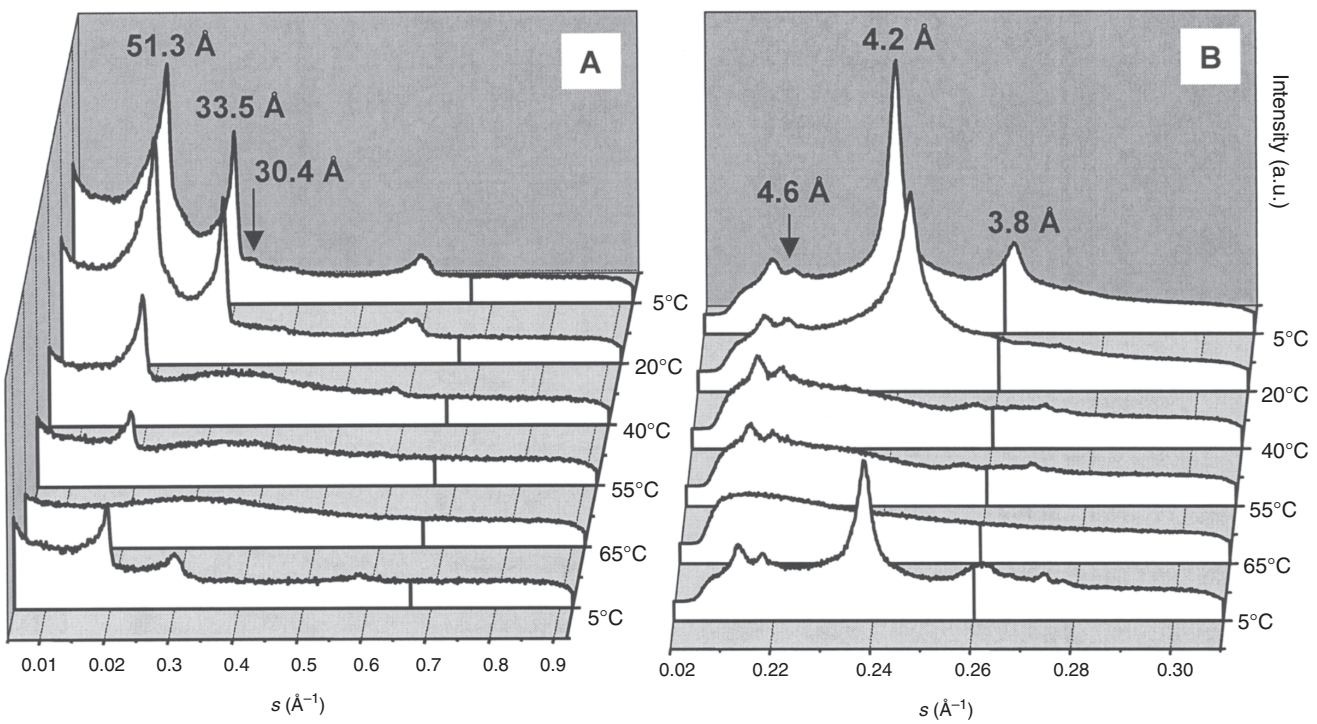

FIG. 3. Small-angle (A) and wide-angle (B) X-ray diffractograms of the solid fraction 6 obtained from heating (5 to 65°C) and cooling (5°C) experiments at the indicated temperatures. $s = h/(2\pi)$ and $h = 4(\pi/\lambda)\sin(\Theta)$, with λ being the wavelength of the X-ray beam and 2Θ the scattering angle.

which were also characteristic of the thermotropic phase behavior of the other samples. In the small-angle region, up to three orders of a lamellar lattice with a lamellar spacing of 51.2 Å could be observed at temperatures between 5 and 55°C and after cooling to 5°C. A second, smaller lamellar lattice with a lamellar spacing of 33.4 Å could be deduced owing to its pronounced first-order reflection and the corresponding second-order reflection at 16.7 Å. The latter partially overlapped with the third-order reflection of the larger lattice (17.1 Å). This lattice, which may have been due to chain interdigitation (described in the following discussion), appeared at temperatures up to 20°C upon heating and again at 5°C after cooling. Upon cooling, the diffractograms showed a lower peak intensity, indicating that the systems were in a less-ordered state but that they annealed after a longer incubation at the low temperature. Finally, the small peak observed at 5°C at 30.4 Å could not be related to a lamellar lattice. The wide-angle diffraction data of fraction 6 (Fig. 3B) indicate that at 5°C, the hydrocarbon chains were packed in an orthorhombic subcell. Coinciding with the endotherm at low temperatures observed by DSC, a rearrangement of the hydrocarbon chains occurred, and the chains were hexagonally packed at 20°C, as indicated by a single symmetrical peak at 4.12 Å. The orthorhombic hydrocarbon chain packing is characteristic of the β′-crystalline phase. However, it is generally accepted that the thermal stability of α-crystals is lower than that of β′-crystals and that β-crystals have the highest m.p. (11). Therefore, the wide-angle diffraction pattern observed at 5°C must have been due to a sub-α-crystalline phase, which transformed to the α-crystalline phase at higher temperatures. Such reversible low-temperature transitions involving a reorganization of the hydrocarbon chains from orthorhombic to hexagonal packing also have been observed in MAG (7), DAG (15), and TAG (11) and are characterized by a small change in heat capacity and no changes in the lamellar repeat distance. Indeed, in our case no significant changes in the long spacings were observed at temperatures below and above this transition. However, at 5°C fraction 6 as well as fraction 7 (see the following discussion) exhibited an additional weak reflection at about 30.5 Å that vanished upon heating to 20°C. The origin of these reflections cannot be explained within the scope of this study. The disappearance of the reflection at 4.12 Å at 40°C was accompanied by a vanishing of the 33.4 Å lattice in the small-angle region, where a broad side maximum occurred instead, indicative of the melting of the α-crystalline phase. Additional reflections at about 4.6–4.7 Å occurred in all wide-angle diffractograms at temperatures up to 55°C. This indicates that part of the sample formed a β-crystalline phase, which seemed to be associated with the larger lamellar lattice, as deduced from the persistence of the first-order reflection at 51.2 Å in this temperature range. Finally, at 65°C the entire sample was in the melted state, where the positional correlation of the lamellar lattice was lost, as demonstrated by the absence of sharp Bragg reflections. Instead, a diffuse scattering with a broad side maximum was observed, indicating the existence of an isotropic liquid phase. Upon cooling to 5°C within 30 min, all spacings initially observed occurred again except for the weak 30.4 Å peak, which may have been due to annealing processes, as already mentioned.

Figure 4A depicts the small-angle diffractograms of all samples recorded at 5°C. The reflections of fractions 6 and 7 were rather sharp, whereas the Bragg peaks in the LFEGPG blend and in fraction 5 were imposed on a diffuse scattering background. Several coexisting lamellar lattices were also observed for the LFEGPG blend sample (Table 4). At 5°C, two orders of a lamellar lattice corresponding to a lamellar spacing of 34.1 Å were detected. Furthermore, the first, third, and fourth orders of a larger lamellar lattice of 61.4 Å were detected. A shoulder occurring at about 54.4 Å was probably part of a broad overlapping peak that could not be correlated to higher orders. Another shoulder occurred at 46.2 Å, and the third-order reflection of this spacing could be seen as well. Upon heating to 20°C, no

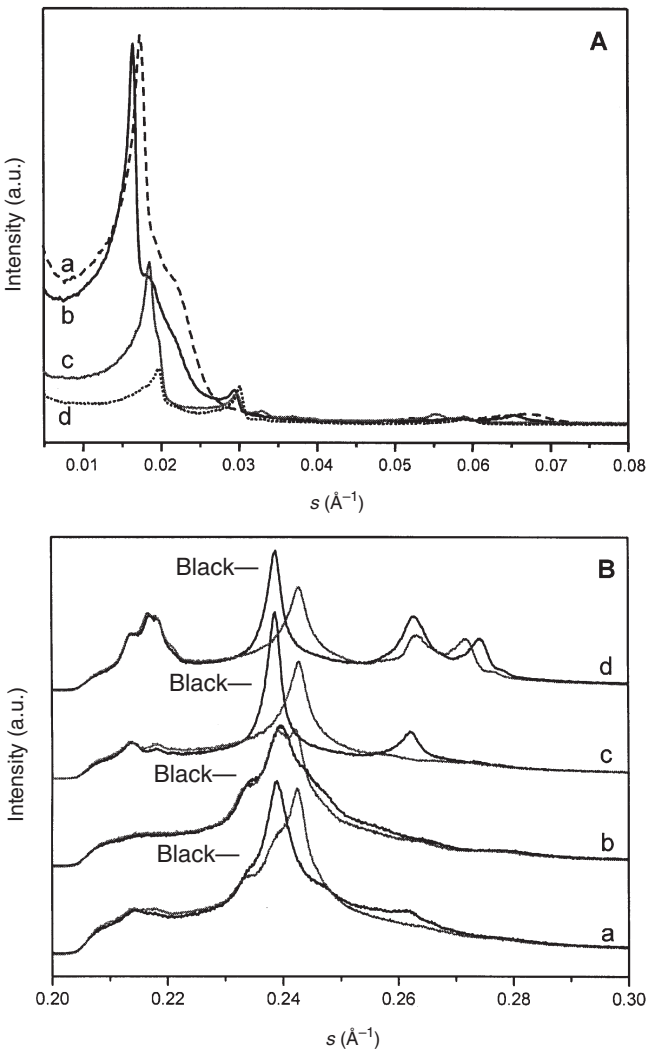

FIG. 4. (A) Small-angle X-ray diffractograms of all samples recorded at 5°C for comparison of the shape of the reflections. (B) Wide-angle X-ray diffractograms recorded at 5°C (black lines) and 20°C (gray lines): LFEGPG (a), fraction 5 (b), fraction 6 (c), fraction 7 (d). For definition of *s* see Figure 3; for abbreviation see Figure 1.

changes were observed in the small-angle region. The wide-angle diffraction patterns recorded at 5 and 20°C are shown in Figure 4B. The diffractogram of the LFEGPG blend at 5°C was characterized by a broad peak at 4.18 Å (with shoulders at approximately 4.27 and 4.04 Å), accompanied by a small peak at 3.82 Å. Upon heating to 20°C, the peak at 3.82 Å disappeared, which mirrored the transition from the sub-α-crystalline to the α-crystalline phase. The weak reflections at 4.6 Å and somewhat smaller scattering angles indicate the existence of a β-crystalline phase throughout the entire temperature range up to the melting temperature.

The shape of the small-angle X-ray diffraction patterns of fraction 5 (Fig. 4A) was similar to that of the LFEGPG blend. At 5°C only two lamellar lattices with lattice spacings of 58.3 and about 46.5 Å were observed. The wide-angle region was dominated by one large reflection at 4.17 Å, with a shoulder at 4.25 Å (Fig. 4B). The positions of the peaks shifted slightly with changing temperatures, but the features remained the same until the m.p. was reached (Table 4). After cooling back to 5°C, only one peak could be observed in the small-angle region. The wide-angle reflection at 4.14 Å showed that again an α-crystalline phase was formed. The absence of peaks at around 4.6 Å was concordant with the DSC data, where only one phase transition attributable to the melting of the α-crystalline phase was observed. Obviously, fraction 5 neither converted to a sub-α-crystalline phase at low temperatures nor formed a stable β-crystalline phase. Very weak reflections at larger scattering angles indicated that small amounts of the sample convert to a β′-crystalline phase. However, no separate phase transition was observed by DSC, which could be attributed to the formation or transition of the β′-crystalline phase.

The reflections of fraction 7 detected in the small-angle region (Fig. 4A, Table 4) gave a picture similar to that of fraction 6. The largest and the smallest lamellar spacings were somewhat larger than those observed in fraction 6. The first- and third-order reflections of a lamellar lattice with a spacing of 51.2 Å were also observed. As in fraction 6, an uncorrelated weak reflection at higher scattering angles could be observed at 5°C. Fraction 7 showed several overlapping peaks in the wide-angle region at about 4.6 Å and smaller scattering angles (Fig. 4B, Table 4). These reflections persisted throughout the entire temperature range of these experiments and reflected the presence of domains in the β-crystalline phase. As seen in the DSC thermogram (Fig. 2), the temperature of the second endotherm was 65.6°C; hence, the complete melting of this fraction could not be observed with X-ray diffraction. At larger scattering angles, we observed several small peaks at 3.80, 3.64, and 3.57 Å that approached each other with increases in temperature. Although the rearrangement of these peaks, which occurred between 5 and 20°C, suggests a sub-α- to α-crystalline phase transition, which is in agreement with the observed DSC data, these peaks persisted (albeit with shifted positions) up to 65°C. At higher temperatures even more weak reflections occurred in this region. Therefore, we suggest that β′-crystals were also formed in this sample.

The DSC and X-ray data show that in all samples, the α-crystalline phase was melting at about 40°C. In the LFEGPG blend and in fractions 6 and 7, the small-angle reflections observed between 51 and 54 Å and the wide-angle reflections, which indicated the β-crystalline phase, remained up to the respective melting temperatures of the β-crystalline phase. The melting temperature of the β-crystalline phase was the lowest for the LFEGPG blend and the highest for fraction 7. This effect shows that in fraction 7, the lipids forming the β-crystalline phase were packed more tightly, resulting in a higher thermal stability of this phase. The transition enthalpies observed with DSC indicate that in the sample of the LFEGPG blend, only a small domain of the entire sample formed such a phase. Also, in fraction 6 the enthalpy observed was comparatively small, whereas in fraction 7 the enthalpy was even larger in the high-temperature transition than in the melting of the α-crystals (see Table 3). The main difference in the sample composition between fractions 6 and 7 was in the number of lactic acid molecules in the head group. It seems that with an increasing number of polymerized lactic acid molecules, the lipid molecules could pack more tightly, probably being supported by attractive interactions between the lactic acid moieties. These interactions between adjacent head groups probably allowed for a closer approach of the hydrocarbon chains and therefore for stronger attractive van der Waals interactions. Such a reorganization of the head group would also explain the increased lattice spacing of fraction 7 compared with fraction 6.

The reason for the occurrence of different long spacings in different samples, all bearing C18:0 and C16:0 hydrocarbon chains, respectively, is difficult to understand. Taking into account the variety of different components in these samples, one can imagine that different arrangements of the single molecules were necessary in the different samples to pack in a sterically acceptable way. Several factors can affect the lattice spacing. One factor could be the conformation of the lipid head group (15), as already mentioned. Another factor might be the mode of hydrocarbon chain packing. In fractions 6 and 7, we observed two different lattice spacings in the small-angle region with a difference in the repeat period of about 20 Å. Because the increment in the lamellar spacing was about 1.3 Å per CH_2-group (15), we assumed that the larger spacings occurred because of a so-called "double-chain-length packing" (2), where the methyl ends of the hydrocarbon chains were opposing in the bilayer, and that the smaller spacing originated from a "single-chain-length packing" (2) because of interdigitated hydrocarbon chains. The single-chain packing reflections, at 33.3 and 33.7 Å, respectively, disappeared at the lower-temperature m.p. and could therefore have been related to the less stable α-crystalline phase. The reflections occurring from the noninterdigitated packing persisted until the thermally more stable β-crystals melted. Interdigitation can release the stress arising from a steric mismatch caused by a large head-group volume and a small hydrocarbon chain volume, as in single-chain lipids, by filling the voids in the hydrocarbon chain moiety. Therefore, we observed the interdigitated hydrocarbon chains in the α-crystalline phase, where the head groups were less tightly packed. The

third factor that affected the lattice spacing was the occurrence of different tilt angles between the hydrocarbons chains and the bilayer plane. Blaurock (11) reported that the tilt angle of the hydrocarbon chains was increased for the β-crystalline phases of fats as compared with the α-crystalline phase. In contrast to hydrated PL, in which the interdigitated phase was observed only with hydrocarbon chains that were perpendicular to the bilayer surface (16), in crystalline phases the interdigitated hydrocarbon chains also could be tilted (17), which increased the number of possible lattice spacings. However, in the LFEGPG blend and in fraction 5, tilted hydrocarbon chains seemed to have a distinct impact on the lattice spacings. This was emphasized by the large full width at half maximum (FWHM) of the wide-angle reflection at 4.2 Å, as the FWHM was related to the sample order (18). In contrast, the spacings at 4.2 Å in fractions 6 and 7 had comparatively small FWHM of 0.003 $Å^{-1}$. This was approximately the same dimension as observed for the interdigitated gel phase of 1,2-distearoyl-*P*-*O*-ethylphosphatidylcholine with stiff and fully extended hydrocarbon chains (19). Therefore, we concluded that the α-crystalline phase of fractions 6 and 7 also had stiff and fully extended hydrocarbon chains that were oriented normally to the bilayer plane, without any tilt angle.

Compared with the "conjoined crystals" (8) that also formed a stable α-crystalline phase at room temperature, LFEGPG exhibited a lower melting temperature. Smaller attractive interactions between the hydrocarbon chains were probably responsible for this effect. It is logical that the nonlactylated head groups of the conjoined crystals were smaller than the lactylated ones of LFEGPG; therefore, a closer approach of the hydrocarbon chains might be realized.

Finally, this study demonstrated that relatively small changes in the polar/apolar interface of a lipid could lead to pronounced effects in the lipid phase behavior. The insight gained into the impact that modified head groups and backbones have on the lipid phase behavior is a prerequisite for realizing food and other technical applications, where tailored lipid mesophases with tuned interfacial characteristics are needed.

ACKNOWLEDGMENTS

We thank Roos Horsten (Unilever R&D Vlaardingen) for performing HPLC measurements and Chris van Platerink and Teun de Joode (Unilever R&D Vlaardingen) for carrying out MS investigations. We are grateful to Richard Koschuch (Institute of Biophysics and X-ray Structure Research, Graz) for helpful suggestions. This work was supported by the European Commission (Marie Curie Industry Host Fellowship, HPMI-GH-01-00116-01).

REFERENCES

1. Garti, N., Delivery of Microparticulated Liquid Systems in Food, in *Handbook of Nonmedical Applications of Liposomes*, edited by Y. Barenholz and D.D. Lasic, CRC Press, Boca Raton, FL, 2000, pp. 143–198.
2. Krog, N.J., Food Emulsifiers and Their Chemical and Physical Properties, in *Food Emulsions*, edited by S.E. Friberg and K. Larsson, Marcel Dekker, New York, 1997, pp. 141–188.
3. El Baraka, M., E.I. Pecheur, D.F. Wallach, and J.R. Philippot, Non-phospholipid Fusogenic Liposomes, *Biochim. Biophys. Acta 1280*:107–114 (1996).
4. Hird, G.S., T.J. McIntosh, A.A. Ribeiro, and M.W. Grinstaff, Synthesis and Characterization of Carbohydrate-Based Phospholipids, *J. Am. Chem. Soc. 124*:5983–5992 (2002).
5. Renzo, D.J., *Doughs and Baked Goods: Chemical, Air, and Non-leavened*, Noyes Data Corporation, Park Ridge, NJ, 1975, pp. 325–357.
6. Martin, J.B., and E.S. Lutton, Preparation and Phase Behavior of Positionally Isomeric Propylene Glycol Monoesters, *J. Am. Oil Chem. Soc. 42*:529–533 (1965).
7. Lutton, E.S., C.B. Stewart, and J.B. Martin, Clarification of Propylene Glycol Monoester Polymorphism, *Ibid. 49*:186–187 (1972).
8. Kuhrt, N.H., R.A. Broxholm, and W.P. Blum, Conjoined Crystals I. Composition and Physical Properties, *Ibid. 40*:725–730 (1963).
9. Reid, E.J., and N.J. Dumont, Emulsifier and Method of Making Same, U.S. Patent 3,158,487 (1964).
10. Laggner, P., and H. Mio, SWAX—A Dual-Detector Camera for Simultaneous Small- and Wide-Angle X-ray Diffraction in Polymer and Liquid Crystal Research, *Nucl. Instrum. Methods Phys. Res. 323*:86–90 (1992).
11. Blaurock, A.E., Fundamental Understanding of the Crystallization of Oils and Fats, in *Physical Properties of Fats, Oils, and Emulsifiers*, edited by N. Widlak, AOCS Press, Champaign, 1999, pp. 1–32.
12. Sonoda, T., Y. Takata, S. Ueno, and K. Sato, 2004. DSC and Synchrotron-Radiation X-ray Diffraction Studies on Crystallization and Polymorphic Behavior of Palm Stearin in Bulk and Oil-in-Water Emulsion States, *J. Am. Oil Chem. Soc. 81:*365–373 (2004).
13. Sato, K., S. Ueno, and J. Yano, Molecular Interactions and Kinetic Properties of Fats, *Prog. Lipid Res. 38*:91–116 (1999).
14. Tardieu, A., V. Luzzati, and F.C. Reman, Stucture and Polymorphism of the Hydrocarbon Chains of Lipids: A Study of Lecithin–Water Phases, *J. Mol. Biol. 75*:711–733 (1973).
15. Di, L., and D.M. Small, Physical Behavior of the Hydrophobic Core Membranes: Properties of 1-Stearoyl-2-Linoleoyl-*sn*-Glycerol, *Biochemistry 34*:16672–16677 (1995).
16. Ranck, J.L., T. Keira, and V. Luzzati, A Novel Packing of the Hydrocarbon Chains in Lipids, *Biochim. Biophys. Acta 488*: 432–441 (1977).
17. Hauser, H., I. Pascher, and S. Sundell, Conformation of Phospholipids. Crystal Structure of a Lysophosphatidylcholine Analogue, *J. Mol. Biol. 137*:249–264 (1980).
18. Blaurock, A.E., Evidence of Bilayer Structure and of Membrane Interaction from X-ray Diffraction Analysis, *Biochim. Biophys. Acta 650*:167–207 (1982).
19. Winter, I., G. Pabst, M. Rappolt, and K. Lohner, Refined Structure of 1,2-Diacyl-*P*-*O*-Ethylphosphatidylcholine Bilayer Membranes, *Chem. Phys. Lipids 112*:137–150 (2001).

[Received June 15, 2004; accepted September 16, 2004]